

## MPOX

# Structure of monkeypox virus DNA polymerase holoenzyme

Qi Peng<sup>1†</sup>, Yufeng Xie<sup>2†</sup>, Lu Kuan<sup>1†</sup>, Han Wang<sup>1,3</sup>, Jianxun Qi<sup>1</sup>, George F. Gao<sup>1,2,4,5,6\*</sup>, Yi Shi<sup>1,5,6\*</sup>

The World Health Organization declared mpox (or monkeypox) a public health emergency of international concern in July 2022, and prophylactic and therapeutic measures are in urgent need. The monkeypox virus (MPXV) has its own DNA polymerase F8, together with the processive cofactors A22 and E4, constituting the polymerase holoenzyme for genome replication. Here, we determined the holoenzyme structure in complex with DNA using cryo-electron microscopy at the global resolution of ~2.8 angstroms. The holoenzyme possesses an architecture that suggests a “forward sliding clamp” processivity mechanism for viral DNA replication. MPXV polymerase has a DNA binding mode similar to that of other B-family DNA polymerases from different species. These findings reveal the mechanism of the MPXV genome replication and may guide the development of anti-poxvirus drugs.

**A**s of 2 December 2022, over 82,000 human mpox (or monkeypox) cases have been laboratory confirmed in 110 countries worldwide (<https://www.cdc.gov/>). Most infection cases have been reported in Europe and other non-endemic countries, including China (1), and these cases were mostly found in homosexual young men (2). Human-to-human transmission usually occurs through close contact with lesions, respiratory droplets, body fluids, and contaminated materials, such as bedding (3).

Although the monkeypox virus (MPXV) was first isolated from a monkey in Denmark in 1958, its natural host was thought to be rodent (3, 4). Since the first human mpox case was identified in the Democratic Republic of the Congo (5), it has been endemic to several central and western African countries (6, 7). Sporadic infection cases have been reported outside Africa, including England, the United States, Singapore, and Israel, and are mainly associated with travelers from endemic countries, nosocomial infections, or direct contact with imported rodents infected with MPXV (4, 8, 9). Phylogenetic analysis has revealed that MPXV can be classified into two genetic clades: the West Africa clade and the more pathogenic Congo Basin clade (10, 11). The 2022 outbreak of MPXV belongs to the West Africa clade and most likely has a single origin that has not been identified (12).

MPXV is a large double-stranded DNA virus that replicates exclusively in the cytoplasm of the infected cells. It belongs to the *Orthopoxvirus* genus of the Poxviridae family, which also includes the variola virus that causes smallpox and has killed millions of humans in recorded history. Similar to the vaccinia virus (VACV), the prototype of poxviruses, MPXV may enter host cells by either fusion with the plasma membrane or endocytosis, and at least 16 proteins in the virion membrane are involved in the entry process (13). After entry, the virus initiates early gene transcription events, and viral DNA synthesis occurs at perinuclear sites called viral factories (14, 15). The MPXV replicative holoenzyme consists of catalytic polymerase F8 (equivalent to E9 in VACV), a heterodimeric processivity factor consisting of A22 (equivalent to A20 in VACV) and uracil-DNA glycosylase E4 (equivalent to D4 in VACV).

Previous genetic, biochemical, and structural studies on the VACV E9-A20-D4 core replication machinery have advanced our understanding of poxvirus DNA replication. VACV E9 was recognized as a member of the B-family DNA polymerase, and structural analysis has revealed the canonical features of DNA polymerases and five poxvirus-specific insertions (16). The E9 polymerase alone does not have processive DNA synthesis activity unless it is bound to its heterodimeric cofactor A20/D4 (17–20). Although poxvirus DNA polymerase shares many features with other B-family polymerases, the processivity factor is distinctive. In VACV, A20 serves as an essential bridge to link E9 and D4 together and shares no homology with viral proteins beyond poxvirus. The N-terminal domain of A20 binds to D4 (21–23), and its C-terminal domain binds to one insertion in the palm domain of E9 (24). Given that the DNA replication machinery is extremely conserved for orthopoxviruses, with a sequence identity of more than 97% between VACV and MPXV, the results obtained

for VACV could also be applied to MPXV. However, we are still awaiting a reliable high-resolution structure of the replicating state of the *Orthopoxvirus* polymerase holoenzyme, and the mode of operation of the processivity factor needs to be elucidated.

## Results

### Biochemical characterization of the purified polymerase proteins

We coexpressed MPXV F8 polymerase and the A22-E4 heterodimer using the baculovirus expression system and purified the homogeneous F8-A22-E4 heterotrimer protein for enzymatic and structural studies (fig. S1). When a 38-nucleotide (nt) template DNA was used with a 24-nt primer DNA, the wild-type holoenzyme heterotrimer displayed weak primer extension activity in the reaction buffer with deoxyribonucleotide triphosphate (dNTP) (fig. S1). Moreover, exonuclease activity was confirmed using an enzymatic assay without dNTP substrates. The holoenzyme could completely degrade the primer DNA in an adenosine 5'-triphosphate (ATP)-independent manner (fig. S1). We also prepared an exonuclease-deficient F8 mutant protein and found that the F8-mutant-A22-E4 holoenzyme did not cleave the primer-template DNA, thereby demonstrating a much stronger product band than the wild-type holoenzyme protein, and the polymerization product could be efficiently inhibited by heparin (fig. S1).

### Overall architecture of F8-A22-E4 polymerase holoenzyme

To capture the replicating conformation of the MPXV F8-A22-E4 polymerase holoenzyme, we incubated the 3'-H modified primer-template DNA and the exonuclease-deficient polymerase holoenzyme in the reaction buffer with deoxythymidine triphosphate (dTTP) substrate. We then prepared cryo-electron microscopy (cryo-EM) samples using a graphene grid to avoid preferential orientation observed with ordinary grids. The holoenzyme–DNA complex was resolved to ~2.8 Å (figs. S2 and S3). The EM map shows the key structural features of all proteins and DNA elements (fig. S4). Although the density of the 5'-end template was weak, we traced the main chains using the unsharpened EM density map to demonstrate the template entry channel (see below).

The structure of the holoenzyme–DNA complex contains one F8, one A22, one E4, and the primer-template DNA, as well as an incoming dTTP substrate (Fig. 1). F8, A22, and E4 form pairwise interactions with each other (Fig. 1).

The F8 structure can be traced for 1004 residues, except for the last two residues, and the classical N-terminal domain (NTD), exonuclease domain (Exo), palm domain, fingers domain, and thumb domain were observed in a closed conformation (Fig. 1). Five “poxvirus-specific” insertion regions in MPXV F8 can also

<sup>1</sup>CAS Key Laboratory of Pathogen Microbiology and Immunology, Institute of Microbiology, Chinese Academy of Sciences, Beijing 100101, China. <sup>2</sup>Department of Basic Medical Sciences, School of Medicine, Tsinghua University, Beijing 100084, China. <sup>3</sup>College of Future Technology, Peking University, Beijing 100871, China. <sup>4</sup>Savard Medical School, University of Chinese Academy of Sciences, Beijing 100049, China. <sup>5</sup>Center for Influenza Research and Early-warning (CASICRE), CAS-TWAS Center of Excellence for Emerging Infectious Disease (CECID), Chinese Academy of Sciences, Beijing 100101, China. <sup>6</sup>Research Unit of Adaptive Evolution and Control of Emerging Viruses, Chinese Academy of Medical Sciences, Beijing 100052, China.

\*Corresponding author. Email: gao@im.ac.cn (G.F.G.); shiyi@im.ac.cn (Y.S.)

†These authors contributed equally to this work.

be observed, like those inserts seen in the VACV E9 structure (16) (Fig. 1 and fig. S5, A and B).

The 218-residue MPXV E4 resembles the VACV D4 structure (25) (Fig. 1A and fig. S5, C and D). The 426-residue MPXV A22 structure can be divided into three domains: the A22 NTD, middle domain (Mid), and C-terminal domain (CTD) (Fig. 1A and fig. S5E). When we aligned the Mid of A22 on the online Dali server, we found that it shows high structural similarities with the African swine fever virus (ASFV) DNA ligase and the bacteriophage T4 DNA ligase (26, 27). The Mid can be further divided into two subdomains: an adenylation domain (OD), which mostly resembles the OD of ASFV DNA ligase (fig. S5F), and an OB-fold domain (OB), which mostly resembles the OB of *Thermus filiformis* DNA ligase (fig. S5G). Further enzymatic assay showed that the MPXV polymerase holoenzyme did not possess ordinary ligase activity similar to that of T4 ligase (fig. S6, A and B). Compared with the structures of adenylation domains from the T4 and ASFV ligases, the putative ligase active site of the A22 Mid is replaced by hydrophobic and negatively charged residues, which may prevent the binding of ATP (fig. S6C). As the Mid of A22 lacks the essential DNA binding domain, A22 may comprise a degenerative ligase domain acting simply as a flexible linker.

The MPXV DNA polymerase holoenzyme is stabilized by pairwise interactions between the F8, A22, and E4 subunits (fig. S7). A22 acts as a bridge to bind E4 and F8 via the A22 NTD and CTD, respectively. The interactions are almost identical to those of their VACV counterparts (fig. S8) (21–24). A previous study proposed a VACV polymerase holoenzyme model with an elongated shape of the A20-D4 cofactor, leading to a ~150-Å distance between the E9 polymerase active site and the D4 DNA binding site (28). However, in our replicating MPXV holoenzyme structure, the A22-E4 cofactor folds back, and E4 directly interacts with the Exo domain of F8 at two sites, one where Trp<sup>36</sup> and Arg<sup>39</sup> of E4 form hydrogen bonds and hydrophobic interactions with Phe<sup>179</sup> and Leu<sup>278</sup> from F8 Exo (fig. S7F), and another where Asn<sup>165</sup> of E4 forms a hydrogen bond with Asn<sup>303</sup> from F8 Exo (fig. S7G).

#### Primer-template DNA recognition by the polymerase complex

The structure of MPXV polymerase holoenzyme-DNA complex contains 22-nt DNA in the template strand, 14-nt DNA in the primer strand, and the incoming dTTP, as well as a magnesium ion that may serve as catalytic ion near the active site (Fig. 2, A and B). The double-stranded primer-template DNA binds in a groove formed between the palm and thumb domains of F8, and the single-stranded 5' extension of the template strand probably passes through a channel formed by the NTD and

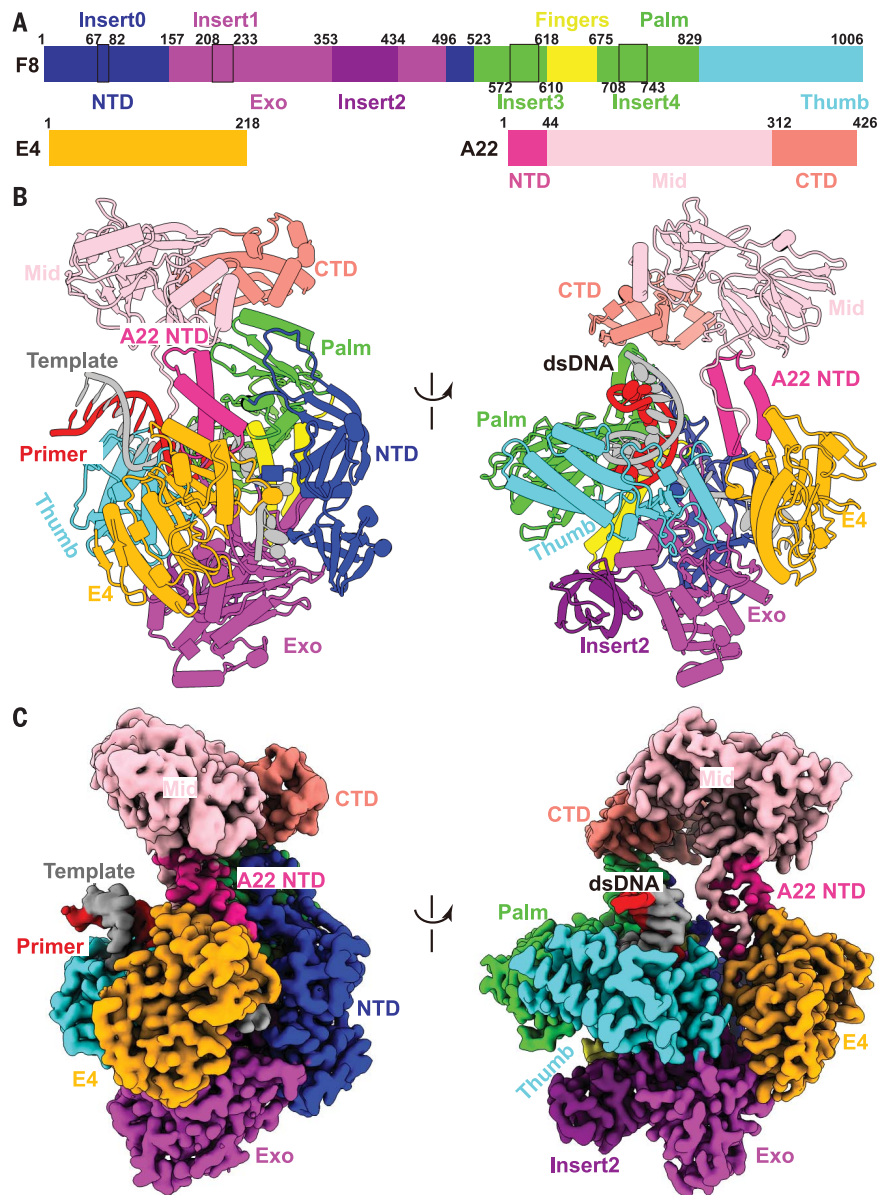


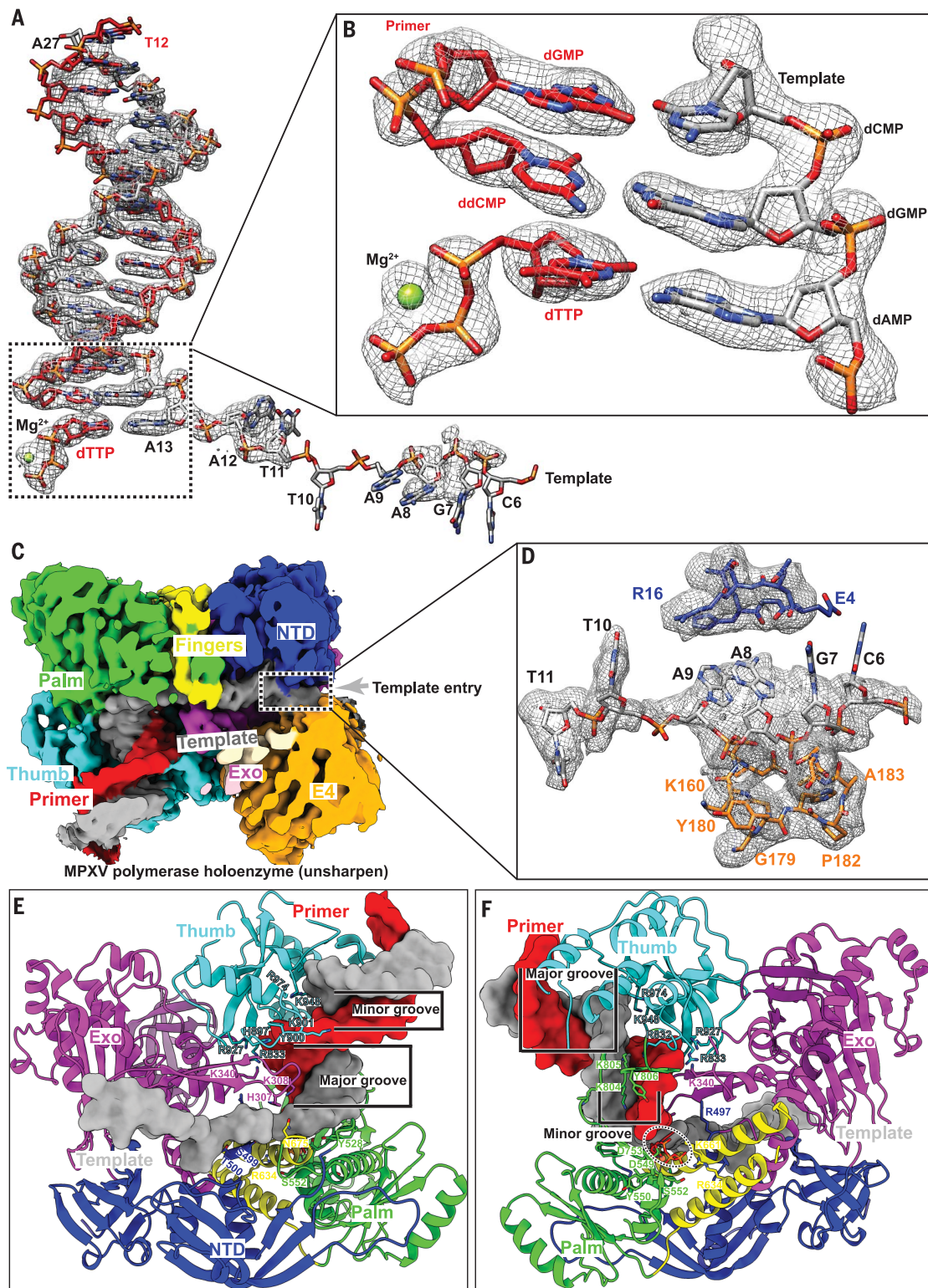
**Fig. 1. Overall structure of the replicating MPXV DNA polymerase holoenzyme.** (A) Schematic diagrams of the domain architecture of MPXV DNA polymerase F8 and processivity factors (A22 and E4). The F8 can be divided into five domains: NTD, blue; Exo, magenta; palm, green; fingers, yellow; thumb, cyan. Compared to other B-family polymerases, F8 contains five inserted elements in which the largest one was named as insert2 (purple), and the other four small inserts are indicated as rectangles. A22 is colored by domains: NTD, deep pink; Mid, pink; CTD, salmon. E4, orange; template strand, gray; primer strand, red. (B and C) Atomic model and cryo-EM density map of the replicating MPXV DNA polymerase holoenzyme. The structures were colored by domains, as depicted in (A).

Exo of F8 and the E4 subunit in an orientation perpendicular to the DNA duplex (Fig. 2, C and D, and fig. S9). The template DNA has 12 unpaired nucleotides at the 5' end, but only two of them are well-ordered with a defined base structure. For the remaining 10 unpaired bases, we can only trace partial phosphate-

ribose backbones (C6 to T11) because of the weak EM density (Fig. 2, C and D).

Upon primer-template DNA binding, F8 polymerase undergoes conformational changes, a common feature of the B-family DNA polymerases. Comparison of the MPXV F8 in this holoenzyme-DNA complex structure with the

**Fig. 2. The interactions between DNA and MPXV polymerase.** **(A)** Sharpened EM densities and atomic models of dsDNA. **(B)** Enlarged view of the sharpened EM densities and atomic models of dsDNA in the active site of polymerase. **(C)** The cut-off view of unsharpened EM density map for MPXV polymerase holoenzyme in complex with the DNA, revealing the consecutive density of template DNA. **(D)** Enlarged view of the unsharpened densities and supposed atomic models of the template DNA in the template entry channel. The region (C6 to T11) was built using this unsharpened map. The remaining 5'-terminal five bases of template DNA were invisible, which reflects an inherent flexible conformation of the 5'-terminal unpaired region of the template strand. **(E and F)** The primary interfaces between F8 and DNA. The F8 mainly interacted with the minor groove of primer-template DNA, with only a few contacts to the major groove contributed by the residues of exonuclease domain. The primer-template DNA is shown in surface representation calculated from the atomic model, and F8 is shown in cartoon representation.



VACV apo E9 structure, which has high sequence identity, shows that the fingers domain rotates toward the palm domain by ~17° in the replicating state (fig. S9). This rotation drags the positively charged Arg<sup>634</sup> and Lys<sup>661</sup> of the fingers domain closer to the active site, where they can interact with the triphosphate group

of incoming dNTP. The rotated fingers domain interacts with the Exo, and this interaction further stabilizes the closed conformation of the fingers domain. Moreover, the thumb domain also makes a distinct rotation to wrap around the primer-template DNA duplex on its minor groove side (fig. S9). The DNA du-

plex is accommodated in a positively charged groove of the thumb domain, as observed in other B-family DNA polymerases (fig. S10).

The modeled double-stranded DNA helix is formed by 14 base pairs from the primer-template DNA and maintains a B-form conformation (Fig. 2A and fig. S11). Extensive

protein-DNA interactions are observed between the primer-template DNA and F8, with a total of 47 residues from F8 directly participating in DNA binding (within 4.0 Å distance, 29 residues to the template strand, and 18 residues to the primer strand) (Fig. 2, fig. S11, and table S2). Most of the key residues involved in primer-template DNA binding are highly conserved among different B-family DNA polymerases. Protein-DNA interactions mainly involve the phosphodiester backbone of the DNA, with many interactions directly with the phosphate groups (fig. S11A). Interactions with the template-strand phosphates are largely hydrogen bonds to the main or side chains of 13 residues from the thumb, palm, fingers domains, Exo, and NTD of F8 (fig. S11, A to C), whereas the primer strand is bound by both electrostatic interactions and hydrogen bonds with the nine residues from the thumb, palm domains, and Exo of F8 (fig. S11, A, D, and E). There is little contact of F8 with the base pairs of primer-template DNA, except for one hydrogen bond interaction between R832 of the thumb domain and the base of T22 from the primer strand, which may be important for stabilizing the B-form conformation of the DNA duplex (fig. S11, A and D). This is consistent with the fact that the enzymatic activity of F8 does not rely on a specific sequence during the elongation step. In addition, residue N675 of the fingers domain forms a hydrogen bond with the base of unpaired A12 from the template strand, and this interaction may be responsible for the kinking of the single-stranded 5' extension of the template strand near the active site.

#### Interactions between the polymerase and the incoming nucleotide

Next to the 3' terminus of the primer strand is the incoming dTTP, which binds to the active site of the polymerase in a manner analogous to that observed in the structures of other DNA polymerase complexes (Fig. 3A) (29). The incoming dTTP is accommodated in a groove formed by residues from the palm and fingers domains (Fig. 3B). The two highly conserved aspartate residues, D549 (in motif A) and D753 (in motif C), together with the triphosphate tail of dTTP, coordinate one divalent metal ion (assumed as magnesium, which has been added to the reaction buffer) (Fig. 3C). The triphosphate tail also interacts with the main chains of Y550, S552, and L553 from motif A, and the side chains of two positively charged R634 and K661 from the fingers domain (Fig. 3C).

The ribose of dTTP stacks on top of the phenyl ring of Y554 from motif A, in a manner similar to that previously observed with Y416 in the ternary complex structure of RB69 polymerase (30) (Fig. 3C). There would be a steric clash between the 2'OH of ribonucleotides and Y554, hence providing a “steric gating” effect

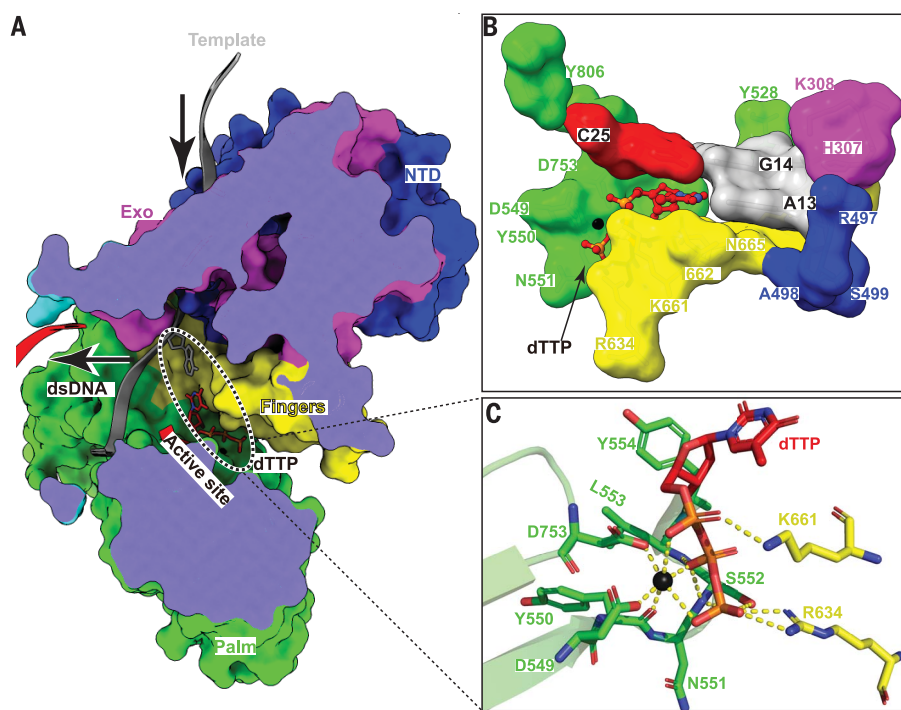


**Fig. 3. Recognition of the incoming dTTP.** (A) Cut-off view of the F8 protein, which is shown in surface representation to reveal the inner active site. The F8 is colored by domains as in Fig. 1; template strand, gray; primer strand, red. (B) The binding pocket of the incoming dTTP. It is formed by the fingers domain, palm domain, and upper base pair. The incoming dTTP is shown as a ball-and-stick model, and the residues of F8 and the upper base pair are shown in surface representation. (C) Interaction details between F8 and the incoming dTTP. The key residues are shown as sticks and colored as corresponding domains. The magnesium ion is depicted as a black sphere. Single-letter abbreviations for the amino acid residues are as follows: A, Ala; C, Cys; D, Asp; E, Glu; F, Phe; G, Gly; H, His; I, Ile; K, Lys; L, Leu; N, Asn; P, Pro; R, Arg; S, Ser; T, Thr; V, Val; W, Trp; and Y, Tyr.

to select dNTP as the substrate. This similar “steric gating” effect has also been described in other DNA polymerases and was first proposed in HIV-1 reverse transcriptase (31–33).

#### Operation mode of processivity cofactor

For B-family DNA polymerases, proliferating cell nuclear antigen (PCNA) or PCNA-like proteins are required for high processivity. However, for poxviruses, including MPXV and VACV, no homologous PCNA-like proteins have been identified in the viral genome. Instead, the poxvirus-specific A22-E4 heterodimer is responsible for the high processivity of DNA replication.

A primer-extension assay using a 60-nt template DNA in the presence of heparin, which can trap the dissociated DNA polymerase from the primer-template DNA to guarantee a single-turnover reaction, showed that the F8 polymerase alone dissociated from the primer-template DNA after incorporating less than 14 nt, whereas the F8-A22-E4 holoenzyme was able to generate full-length 60-nt products with few abortive ones (Fig. 4A). We then demonstrated that the addition of the A22-E4 heterodimer conferred processivity to F8 in a concentration-dependent manner (Fig. 4A). When the molar

ratio of A22-E4 to F8 was 1:1, corresponding to the stoichiometry of the polymerase holoenzyme, the amount of the full-length product was almost the same as that of the product generated by the preassembled F8-A22-E4 polymerase holoenzyme (Fig. 4A). This indicates that the isolated A22-E4 and F8 can be efficiently assembled into functional holoenzymes to perform processive DNA synthesis. Moreover, we performed alanine scanning of critical residues responsible for the interaction between E4 and F8 and found that R39A and N165A substitutions of E4 showed minor effect, W36A reduced the synthesis of full-length products, whereas the W36A/R39A and W36A/R39A/N165A substitutions abolished the synthesis of full-length products (Fig. 4B). These results further confirmed the important function of the A22-E4 heterodimer in DNA replication processivity in a pure enzymatic reaction system.

As described above, the E4 cofactor interacts with the Exo of F8 polymerase, and together with the NTD of F8, they form a closed-ring channel to encircle the single-stranded template DNA (Fig. 4C). By contrast, in the yeast DNA polymerase complex (29), a representative of the other B-family DNA polymerases (fig. S12),

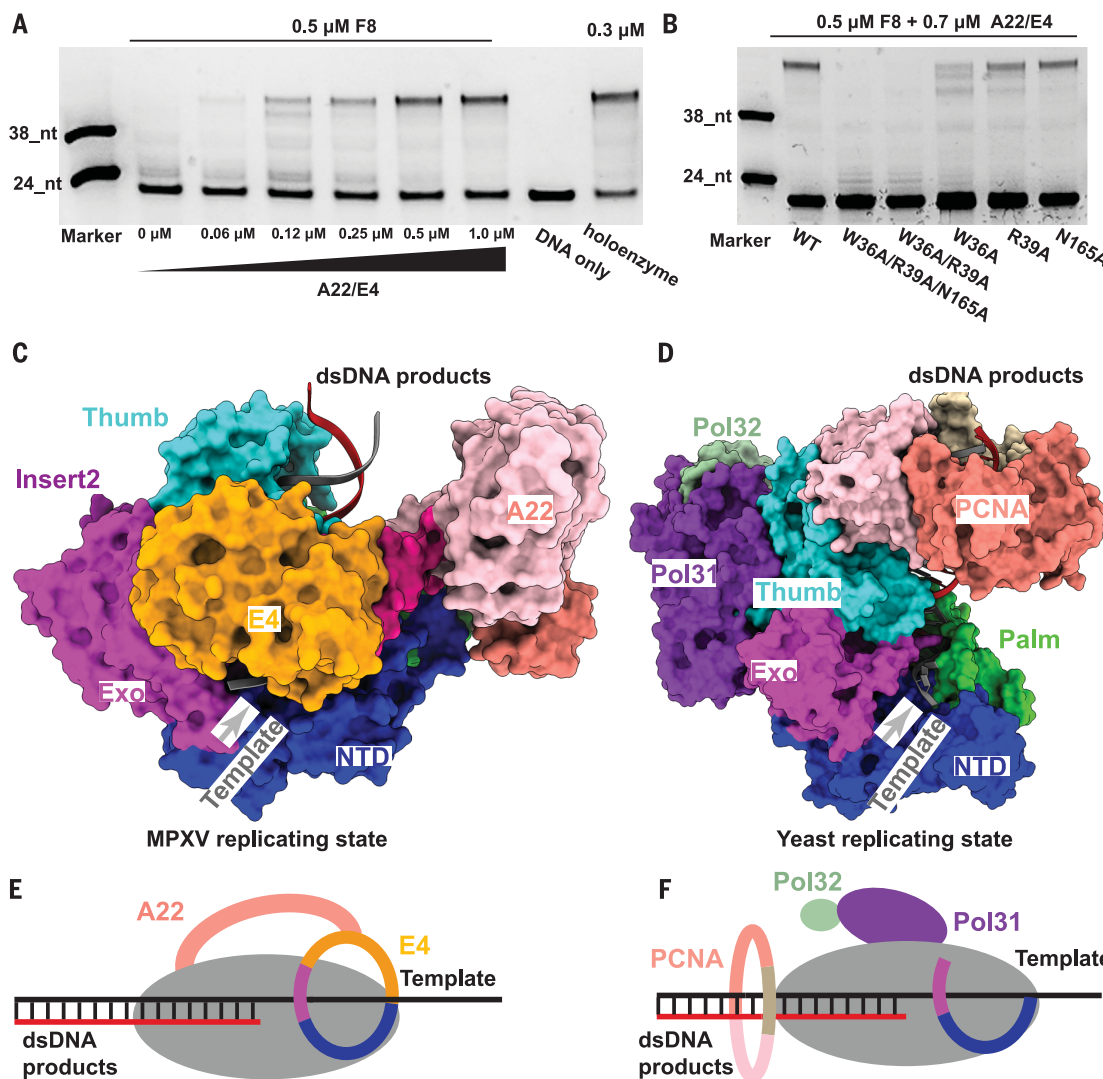


**Fig. 4. The distinctive mechanism of A22-E4 heterodimer promoting processivity of MPXV DNA polymerase.** (A) Enzymatic assay of A22-E4 heterodimer protein improving the DNA replication processivity of exonuclease-deficient F8 under single-turnover conditions. The F8 alone was shown to be distributive and failed to generate full-length products, whereas the addition of the A22-E4 complex promoted the yield of full-length DNA in a concentration-dependent manner. (B) Alanine scanning of critical residues of E4 responsible for the interaction with F8 was performed to examine the effects on the DNA replication processivity. The A22-E4 W36A mutant reduced the processivity activity, whereas the W36A/R39A and W36A/R39A/N165A mutants abolished the processivity activity. The F8 used in this assay was exonuclease deficient. (C and D) Comparison of the structures of the MPXV and yeast polymerases (PDB ID: 7KCO) in complex with their

own processivity factors and DNA. Polymerases and processivity factors are shown in surface representation and colored by domains, as in Fig. 1, whereas the primer-template DNA strands are shown as a cartoon (template, gray; primer, red). The processivity of yeast polymerase was strengthened by trimeric PCNA to clamp the primer-template dsDNA. While in the structure of MPXV polymerase holoenzyme, A22-E4 heterodimer does not interact with dsDNA. Instead, E4 located on the template entry channel combined with NTD and Exo domains of F8 to form a forward clamp structure that would prevent the template strand disassociating from the polymerase complex during DNA replication. (E and F) Two binding modes of processivity factors with polymerases. The processivity factors bound with template in poxvirus function as a “forward sliding clamp” (E) or dsDNA products in eukaryotes as a “backward sliding clamp” (F).

the Exo and NTD form an open semicircular channel to accommodate the single-stranded template DNA, and the trimeric PCNA ring encircles the template-product DNA duplex (Fig. 4D). This architectural difference between MPXV and yeast polymerase complexes is responsible for the different processivity mechanisms during DNA replication events. The MPXV DNA polymerase holoenzyme guarantees its high DNA replication processivity by encircling the single-stranded template

DNA, and we propose that it functions as a “forward sliding clamp” (Fig. 4E); whereas the other B-family DNA polymerase complexes possess continuous DNA replication capacity by encircling the double-stranded template-product DNA helix that can be recognized as a “backward sliding clamp” (Fig. 4F).

#### Discussion

The interaction between E4 and F8 could generate a ring channel that encircles the single-

stranded template DNA, which is proposed to be important for high DNA replication processivity. This processivity mechanism is different from that of other B-family DNA polymerases that utilize PCNA or PCNA-like proteins to encircle the product-template DNA duplex (29, 34, 35). The configuration of encircling the single-stranded template DNA probably allows the MPXV polymerase complex to perform continuous DNA replication by preventing template DNA disassociation from

the polymerase holoenzyme. The efficiency of polymerase holoenzyme assembly in the cellular environment requires further study, and moreover, it should be investigated whether the F8-A22-E4 polymerase holoenzyme has other active conformations (28).

Previous studies have implicated the distinctive role of the polymerase holoenzyme in DNA recombination, which involves both 3'-5' exonuclease and DNA-joining activities (36–38). Although we identified DNA ligase-like domains for the Mid of the poxvirus-specific cofactor A22, the F8-A22-E4 polymerase holoenzyme did not have canonical ligase activity in our assay. However, we cannot rule out the possibility that A22 possesses ligase activity in a different state from the current holoenzyme structure or in an ATP-independent manner. Orthopoxviruses encode a DNA ligase that is not essential for virus replication but affects virulence and sensitivity to DNA-damaging agents (39). Further functional dissection of the middle part of A22 and its cooperation with viral and host ligases is needed.

Poxvirus replication processes use different replication models, including self-priming, primer-dependent, and recombination models (45). Poxviruses, including MPXV, have linear double-stranded DNA genomes, and the termini of the two DNA strands are connected to form a continuous polynucleotide chain (40). A rolling cycle mechanism has been proposed to replicate DNA in the form of unbranched head-to-tail concatemers, which would be resolved by a Holliday junction resolvase to produce unit genomes (41). The proposed “forward sliding clamp” mode can help interpret the self-priming model, as the processivity cofactor would facilitate robust continuous replication along the single-stranded template DNA unwound by the primase-helicase. Because there is also a possible presence of Okazaki fragments for *Orthopoxvirus* DNA replication (42), other replication models should also be

studied. Moreover, the working mechanism of an intact replisome, including the F8-A22-E4 holoenzyme and other replication proteins, will be a fascinating area for future studies.

#### REFERENCES AND NOTES

- H. Zhao et al., *China CDC Wkly.* **4**, 853–854 (2022).
- J. G. Rizk, G. Lippi, B. M. Henry, D. N. Forthal, Y. Rizk, *Drugs* **82**, 957–963 (2022).
- J. Kaler, A. Hussain, G. Flores, S. Kheiri, D. Desrosiers, *Cureus* **14**, e26531 (2022).
- D. Focosi, F. Novazzi, A. Baj, F. Maggi, *Rev. Med. Virol.* **32**, e2392 (2022).
- D. B. Di Giulio, P. B. Eckburg, *Lancet Infect. Dis.* **4**, 15–25 (2004).
- E. M. Bunge et al., *PLOS Negl. Trop. Dis.* **16**, e0010141 (2022).
- W. Tan, G. F. Gao, *China CDC Wkly.* **4**, 847–848 (2022).
- N. Erez et al., *Emerg. Infect. Dis.* **25**, 980–983 (2019).
- A. Vaughan et al., *Euro Surveill.* **23**, 1800509 (2018).
- N. Chen et al., *Virology* **340**, 46–63 (2005).
- A. M. McCollum, I. K. Damon, *Clin. Infect. Dis.* **58**, 260–267 (2014).
- J. Isidro et al., *Nat. Med.* **28**, 1569–1572 (2022).
- B. Moss, *Semin. Cell Dev. Biol.* **60**, 89–96 (2016).
- M. D. Greseth, P. Traktman, *Annu. Rev. Virol.* **9**, 239–259 (2022).
- B. Moss, *Cold Spring Harb. Perspect. Biol.* **5**, a010199 (2013).
- N. Tarbouriech et al., *Nat. Commun.* **8**, 1455 (2017).
- E. S. Stanitsa, L. Arps, P. Traktman, *J. Biol. Chem.* **281**, 3439–3451 (2006).
- A. M. Druck Shudofsky, J. E. Silverman, D. Chattopadhyay, R. P. Ricciardi, *J. Virol.* **84**, 12325–12335 (2010).
- M. W. Czarnecki, P. Traktman, *Virus Res.* **234**, 193–206 (2017).
- K. A. Boyle, E. S. Stanitsa, M. D. Greseth, J. K. Lindgren, P. Traktman, *J. Biol. Chem.* **286**, 24702–24713 (2011).
- C. Contesto-Richefeu et al., *Acta Crystallogr. F Struct. Biol. Commun.* **72**, 687–691 (2016).
- W. P. Burmeister et al., *J. Biol. Chem.* **290**, 17923–17934 (2015).
- C. Contesto-Richefeu et al., *PLOS Pathog.* **10**, e1003978 (2014).
- B. Bersch, N. Tarbouriech, W. P. Burmeister, F. Iseni, *J. Mol. Biol.* **433**, 167009 (2021).
- N. Schormann et al., *BMC Struct. Biol.* **7**, 45 (2007).
- K. Shi et al., *Nucleic Acids Res.* **46**, 10474–10488 (2018).
- Y. Chen et al., *Nat. Commun.* **10**, 387 (2019).
- C. Sèle et al., *J. Virol.* **87**, 1679–1689 (2013).
- F. Zheng, R. E. Georgescu, H. Li, M. E. O'Donnell, *Proc. Natl. Acad. Sci. U.S.A.* **117**, 30344–30353 (2020).
- M. C. Franklin, J. Wang, T. A. Steitz, *Cell* **105**, 657–667 (2001).
- A. P. Silverman, S. J. Garforth, V. R. Prasad, E. T. Kool, *Biochemistry* **47**, 4800–4807 (2008).
- G. J. Klarmann et al., *Biochemistry* **46**, 2118–2126 (2007).
- G. Gao, M. Orlova, M. M. Georgiadis, W. A. Hendrickson, S. P. Goff, *Proc. Natl. Acad. Sci. U.S.A.* **94**, 407–411 (1997).
- Y. Shamoo, T. A. Steitz, *Cell* **99**, 155–166 (1999).
- C. Lancey et al., *Nat. Commun.* **11**, 1109 (2020).
- D. B. Gammon, D. H. Evans, *J. Virol.* **83**, 4236–4250 (2009).
- M. D. Hamilton, A. A. Nuara, D. B. Gammon, R. M. Buller, D. H. Evans, *Nucleic Acids Res.* **35**, 143–151 (2007).
- M. D. Hamilton, D. H. Evans, *Nucleic Acids Res.* **33**, 2259–2268 (2005).
- S. M. Kerr et al., *EMBO J.* **10**, 4343–4350 (1991).
- O. Faye et al., *Lancet Infect. Dis.* **18**, 246 (2018).
- N. Sklenovská, in *Animal-Origin Viral Zoonoses*, Y. S. Malik, R. K. Singh, K. Dhami, Eds. (Springer Singapore, Singapore, 2020), pp. 39–68.
- M. Esteban, J. A. Holowczak, *Virology* **78**, 57–75 (1977).

#### ACKNOWLEDGMENTS

We thank X.L., Y.M., and X.B. at the cryo-EM Center, Shanxi Academy of Advanced Research and Innovation, for their technical support of the cryo-EM data collection. **Funding:** National Key Research and Development Program of China grant 2021YFC2300700 (Y.S.); Strategic Priority Research Program of CAS grant XDB29010000 (Y.S., G.F.G.); National Natural Science Foundation of China (NSFC) grants 82241076, 81871658, 32192452, and 32100119 (Y.S., Q.P.); The Youth Innovation Promotion Association of CAS grant Y201921 (Y.S.).

**Author contributions:** Conceptualization: Y.S., G.F.G., Q.P. Investigation: L.K., Q.P., Y.X., J.Q., H.W. Visualization: Q.P., Y.X., L.K. Funding acquisition: Y.S., G.F.G., Q.P. Supervision: Y.S., G.F.G. Writing – original draft: Y.S., Q.P., G.F.G. Writing – review and editing: Y.S., Q.P., G.F.G. **Competing interests:** The authors declare that they have no competing interests. **Data and materials availability:** Cryo-EM map is available in the Electron Microscopy Data Bank with code EMD-34731. Structural model is available in the Protein Data Bank (PDB) with accession code 8HG1. All materials are available from the authors on reasonable request with materials transfer agreements (MTAs).

**License information:** Copyright © 2023 the authors, some rights reserved; exclusive licensee American Association for the Advancement of Science. No claim to original US government works. <https://www.science.org/about/science-licenses-journal-article-reuse>. In the interest of rapid dissemination of results with immediate public health relevance, the author will make the Author Accepted Manuscript (AAM) version available under a CC BY public copyright license.

#### SUPPLEMENTARY MATERIALS

[science.org/doi/10.1126/science.adc6360](https://science.org/doi/10.1126/science.adc6360)

Materials and Methods

Figs. S1 to S12

Tables S1 and S2

References (43–53)

MDAR Reproducibility Checklist

[View/request a protocol for this paper from Bio-protocol.](https://bio-protocol.org)

Submitted 29 August 2022; accepted 5 December 2022

Published online 15 December 2022

10.1126/science.adc6360